

# Conformal dimensions via large charge expansion

Debasish Banerjee,<sup>1,\*</sup> Shailesh Chandrasekharan,<sup>2,†</sup> and Domenico Orlando<sup>3,‡</sup>

<sup>1</sup>NIC, DESY, Platanenallee 6, D-15738 Zeuthen, Germany

<sup>2</sup>Department of Physics, Duke University, Durham, North Carolina 27708, USA

<sup>3</sup>Albert Einstein Center for Fundamental Physics, Institute for Theoretical Physics, University of Bern, Sidlerstrasse 5, CH-3012, Bern, Switzerland

We construct an efficient Monte Carlo algorithm that overcomes the severe signal-to-noise ratio problems and helps us to accurately compute the conformal dimensions of large- $Q$  fields at the Wilson–Fisher fixed point in the  $O(2)$  universality class. Using it we verify a recent proposal that conformal dimensions of strongly coupled conformal field theories with a global  $U(1)$  charge can be obtained via a series expansion in the inverse charge  $1/Q$ . We find that the conformal dimensions of the lowest operator with a fixed charge  $Q$  are almost entirely determined by the first few terms in the series.

Conformal field theories (CFTs) occupy a central place in our understanding of modern physics. They describe critical phenomena in condensed matter physics and statistical models [1], quantum gravity via the AdS/CFT correspondence [2] and are generically found at fixed points of renormalization group flows [3]. They are uniquely described by a set of dimensionless numbers (the CFT data), *i.e.* conformal dimensions and OPE coefficients associated with the primary fields of the theory. Since they are typically strongly coupled and lack a characteristic scale, it is often difficult to compute the conformal dimensions analytically. Still, a number of sophisticated techniques have been developed to deal with this challenge, both perturbatively (*e.g.*  $4 - \epsilon$  expansion, fixed-dimension expansion, large- $N$ ; see [4] for a review) and non-perturbatively (*e.g.* bootstrap [5]). In some cases Monte Carlo techniques offer a reliable numerical approach for computing the conformal dimensions [6, 7].

Energies of low-lying states also capture universal features of a  $2 + 1$  dimensional CFT when the theory is studied on a space-time manifold  $\mathbb{R} \times \Sigma$  (see [8, 9] for some recent work in this direction). For example conformal dimensions  $D$  of operators on  $\mathbb{R}^3$  are related to the energies  $E_{S^2}$  of states living on a two-sphere of radius  $r_0$  through the relation  $D = r_0 E_{S^2}$  [10, 11]. This relation, known as the state-operator correspondence, is a consequence of the fact that  $\mathbb{R}^3$  is conformally equivalent to  $\mathbb{R} \times S^2(r_0)$ . Recently, such a connection has been used in CFTs with global  $U(1)$  charges to show that the conformal dimension  $D(Q)$  of the lowest operator with fixed  $U(1)$  charge  $Q$  can be expanded in inverse powers of the charge density on a unit sphere  $Q/4\pi$  [12, 13] (see also [14–18] for related work):

$$D(Q) = \sqrt{\frac{Q^3}{4\pi}} \left( c_{\frac{3}{2}} + c_{\frac{1}{2}} \left( \frac{4\pi}{Q} \right) + \dots \right) + c_0 + \mathcal{O}\left(\frac{1}{Q}\right) \quad (1)$$

where  $c_0 \approx -0.093$  and the other coefficients only depend on the universality class. While a simple dimensional analysis allows one to predict the leading large- $Q$  behavior, it is a priori unclear if a power series can capture the

sub-leading corrections. The recent work argues that by separating the theory into sectors of fixed charge  $Q$  one can construct an effective field theory in each sector, which can be used to compute the energies as a power series in  $1/Q$ . Through the state-operator correspondence one can then obtain the series expansion of the conformal dimension  $D(Q)$  and relate directly the coefficients in Eq. (1) to the coefficients in the energy expansion.

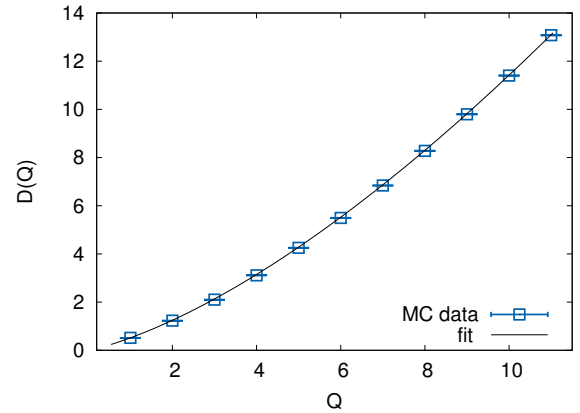


FIG. 1. Plot of the values of  $D(Q)$  extracted from our Monte Carlo calculations at the  $O(2)$  Wilson–Fisher fixed point, along with the plot of Eq. (1) (solid line) with our estimated values  $c_{\frac{3}{2}} = 1.197$  and  $c_{\frac{1}{2}} = 0.077$  and previously computed value  $c_0 = -0.093$ . It is surprising that these three leading coefficients in Eq. (1) can predict the conformal dimensions for all  $Q \geq 1$  very well.

In this work we make significant progress in establishing Eq. (1) by overcoming severe signal-to-noise ratio problems in Monte Carlo methods that had hindered calculations of  $D(Q)$  for large values of  $Q$ . Our new approach allows us to check Eq. (1) and hence determine the coefficients  $c_{\frac{3}{2}}$ ,  $c_{\frac{1}{2}}$ . In Fig 1 we demonstrate this by plotting the measured values of  $D(Q)$  using our Monte Carlo approach together with the plot of Eq. (1) with our predicted values of  $c_{\frac{3}{2}}$  and  $c_{\frac{1}{2}}$  and previously computed value of  $c_0$ . Surprisingly, we find that the large- $Q$

expansion with the first three coefficients predicts the conformal dimensions even at  $Q = 2$  within a few percents. Thus, our work demonstrates that a strongly-coupled conformal fixed point can be described within a simple perturbative framework of effective field theories using  $U(1)$  global charges. In particular, it can provide a complementary method to the numerical bootstrap, since it is most reliable in the regime where the numerical bootstrap becomes technically very challenging and agrees where the two approaches overlap.

To see how all this works, consider the conformal field theory describing the Wilson–Fisher fixed point in the three-dimensional  $O(2)$  universality class. In a fixed charge sector  $Q$ , the charge density introduces the mass scale  $\sqrt{Q/V}$  in the theory and hence for momentum scales  $p \ll \sqrt{Q/V}$  the physics must be describable by the most general scale, Lorentz and  $O(2)$  invariant Lagrangian given by

$$L = \frac{1}{2} \partial_\mu \rho \partial^\mu \rho + \frac{b^2}{2} \rho^2 \partial_\mu \chi \partial^\mu \chi - \frac{R}{16} \rho^2 - \frac{\lambda}{6} \rho^6, \quad (2)$$

where  $\rho$  is the radial field and  $\chi$  is the angular field. The term  $(R/16)\rho^2$  is the conformal coupling of the field  $\rho$  and  $R$  is the scalar curvature of the manifold  $\mathbb{R} \times \Sigma$ . In the large- $Q$  limit only two parameters  $\lambda$  and  $b$  play an important role and all higher derivative terms are suppressed [13, 15].

Using the effective quantum Hamiltonian arising from Eq. (2), one can show that the total energy of the system is given by

$$E_\Sigma(Q) = \sqrt{\frac{Q^3}{V}} \left( c_{\frac{3}{2}} + c_{\frac{1}{2}} \left( \frac{RV}{2Q} \right) + \dots \right) + q_\Sigma + \mathcal{O}\left(\frac{1}{Q}\right), \quad (3)$$

where the first two terms are related to the couplings in the effective Lagrangian Eq. (2) through the relations  $\lambda = 3/2c_{\frac{3}{2}}/(8c_{\frac{1}{2}})^3$  and  $b^2 = 1/(12c_{\frac{1}{2}}c_{\frac{3}{2}})$ . The higher order terms in the expansion are related to higher dimensional operators in Eq. (2) and quantum corrections, which we drop. The last term  $q_\Sigma$  arises due to quantum fluctuations that can be computed exactly for simple manifolds. For the sphere ( $R = 2/r_0^2$ ) one finds  $q_{S^2} = c_0/r_0$  where  $c_0 \approx -0.093$  [14, 19], while for the torus ( $R = 0$ ) it is  $q_{T^2} = c_0/L$  with  $c_0 \approx -0.508$  [20]. By choosing  $\Sigma = S^2$  and using state operator correspondence one can easily derive (1). It is interesting to note that the coefficients  $c_{\frac{3}{2}}$ ,  $c_{\frac{1}{2}}$  in Eq. (1) and (3) are related to the low-energy constants  $\lambda$  and  $b$  of the effective Lagrangian Eq. 2. Indeed, these low-energy constants are independent of the manifold chosen and depend only on the CFT. Assuming the manifold is the torus we predict that

$$\lim_{Q \rightarrow \infty} \frac{D(Q)}{E_{T^2}(Q)L} = \frac{1}{2\sqrt{\pi}}. \quad (4)$$

Note that every term in the energy expansion is a dimensionless function of three variables: a coefficient in the

$D(Q)$  expansion, a geometrical term from the manifold, and a power of  $V/Q$ .

The motivation of our current work is to compute  $D(Q)$  and  $E_\Sigma(Q)$  in the classical  $O(2)$  sigma model on a torus and verify the expansions in Eq. (1) and (3) and the connections between them. We accomplish this by regularizing the classical  $O(2)$  sigma model on a cubic lattice with lattice spacing  $a$  and use Monte Carlo methods to perform the calculations. The model is defined by phases,  $\exp(i\theta_x)$  on each three-dimensional lattice site  $\mathbf{x} = (x_1a, x_2a, x_3a)$  and the nearest neighbor action

$$S = -\beta \sum_{\mathbf{x}, \alpha} \cos(\theta_{\mathbf{x}} - \theta_{\mathbf{x} + \hat{\alpha}a}). \quad (5)$$

Here  $\hat{\alpha}a$  denotes the three unit lattice vectors, and  $\beta$  is the coupling of the model. The physics of the Wilson–Fisher fixed point can be studied by tuning the coupling to its critical value ( $\beta_c = 0.45421$  [21]), where a second-order phase transition separates the symmetric phase ( $\beta < \beta_c$ ) and the spontaneously broken superfluid phase ( $\beta > \beta_c$ ).

Configurations that contribute to the partition function of the lattice model at the critical point can be efficiently generated by both the Wolff cluster algorithm [22] and the worm algorithm based on the worldline representation [23]. However, in order to compute the conformal dimension  $D(Q)$  in  $\mathbb{R}^3$  we need to compute the two-point correlation function  $C_Q(r)$  of charge  $Q$  fields on a large lattice of size  $L$ , which is expected to decay as a power law for large separations  $r \ll L$  at the critical point:

$$C_Q(r) = \langle \exp(iQ\theta_r) \exp(-iQ\theta_0) \rangle \sim \frac{a(Q)}{|\mathbf{r}|^{2-D(Q)}}. \quad (6)$$

Fitting the data to this form we can in principle extract  $D(Q)$  and thus verify Eq. (1). Note that for  $Q = 1$ , it reduces to the standard 2-point correlation function, which is used to extract the critical exponent  $\eta$  through the relation  $C_1(r) = G(r) \propto 1/r^{d-2+\eta}$ . For  $Q = 2, 3, 4$ , the corresponding conformal dimensions have also been computed earlier using different methods, and the results are summarized in table I. Unfortunately, calculations of  $D(Q)$  for higher values of  $Q$  do not exist and hence the relation (1) remains unconfirmed.

$Q$	$\epsilon^5$	$\lambda^6$	MC	bootstrap
1	0.518(1)	-	0.5190(1)	0.5190(1)
2	1.234(3)	1.23(2)	1.236(1)	1.236(3)
3	2.10(1)	2.10(1)	2.108(2)	-
4	3.114(4)	3.103(8)	3.108(6)	-

TABLE I. Conformal dimensions  $D(Q)$  obtained previously by other methods for  $Q \leq 4$ : Field theory results in 4- $\epsilon$  dimensions at five loops are in column two, six loop results at  $d = 3$  are in column three ([24] for  $Q = 2$ , in [25] for  $Q = 3$  and in [26] for  $Q = 4$ ), previous MC results are in column four [21], and bootstrap results are in column five [27].

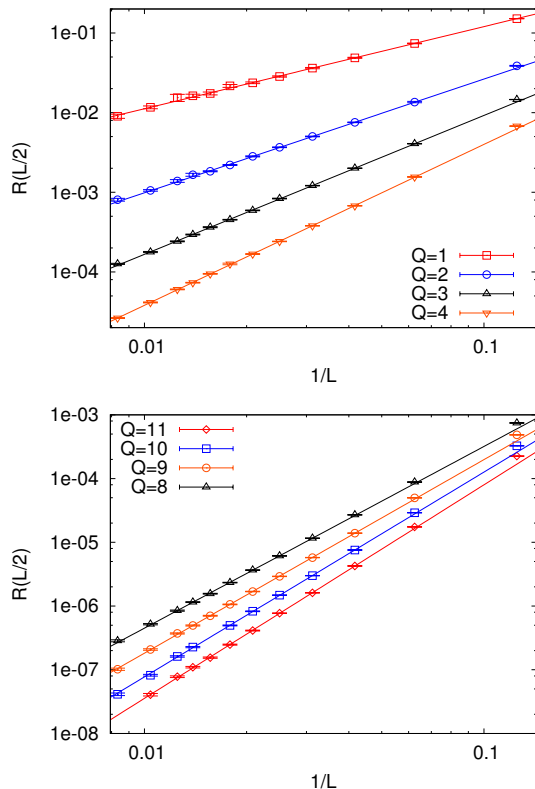


FIG. 2. The figures (top and bottom) show the quantity  $R(L/2)$  for different lattice sizes  $L/a = 8, \dots, 120$  and different  $Q$  values. The straight line on a log-log plot is indicative of the power law behavior, and the slope gives the difference of the conformal dimensions  $2(D(Q+1) - D(Q))$ . Note that there is no visible signal-to-noise problem in these correlators.

It is difficult to measure  $D(Q)$  for large values of  $Q$  through a Monte Carlo method due to severe signal-to-noise ratio problems in the Monte Carlo calculations. With the Wolff cluster algorithm one is averaging numbers of order one with fluctuating signs to compute a small value of  $C_Q(r)$  at large separations. In contrast, in the worm algorithm, one has to build the correct worldline configurations that contribute to the correlation function in the presence of charged sources  $Q$  and  $-Q$  separated by a large distance. In this case the severe signal-to-noise ratio problem emerges as an overlap problem between the vacuum ensemble and the one containing the sources. In order to overcome this problem we have designed an algorithm to efficiently compute the ratio

$$R(L/2) = \frac{C_Q(r = L/2)}{C_{Q-1}(r = L/2)} \quad (7)$$

on cubic lattices of side  $L$  for  $8 \leq L/a \leq 120$  at the critical point  $\beta_c$  (the details of our algorithm can be found in the supplementary material). Using  $R(L/2)$  it is easy to extract the difference  $D(Q) - D(Q-1)$  using the relation  $R(L) \sim 1/L^{2(D(Q) - D(Q-1))}$ . The accuracy

with which we are able to compute the ratio  $R(L/2)$  for various values of  $Q$  can be seen in Fig. 2. Once the differences  $D(Q) - D(Q-1)$  are known, we can also extract  $D(Q)$  by setting  $D(Q=0) = 0$ . Our estimates of both  $D(Q) - D(Q-1)$  and  $D(Q)$  using Monte Carlo calculations, are given in table II. It is easy to verify that our results match quite well with previous results in table I when  $Q \leq 4$ .

$Q$	$D(Q) - D(Q-1)$	$D(Q)$
1	0.516(2)	0.516(2)
2	0.714(5)	1.230(5)
3	0.872(3)	2.101(6)
4	1.010(2)	3.111(7)
5	1.141(5)	4.252(8)
6	1.243(3)	5.494(8)
7	1.346(5)	6.840(10)
8	1.438(4)	8.278(10)
9	1.519(4)	9.796(11)
10	1.607(6)	11.40(1)
11	1.675(5)	13.08(1)

TABLE II. Results for the conformal dimension  $D(Q)$  defined through (6). Our results for  $Q \leq 4$  are in agreement with previous results as seen in table I.

We can now verify if the conformal dimensions in table II are consistent with Eq. 1. For this purpose we perform a combined fit of our data for the difference  $D(Q) - D(Q-1)$  and  $D(Q)$  assuming that  $c_{3/2}, c_{1/2}, c_{-1/2}$  are non-zero and  $c_0 = -0.093$  as expected. Taking into account various systematic errors from fitting procedures we estimate  $c_{3/2} = 1.194(10)$ ,  $c_{1/2} = 0.077(10)$  and  $c_{-1/2} = -0.0014(20)$ . The raw data for  $D(Q) - D(Q-1)$  are shown in Fig. 3. We also show a comparison with the prediction obtained by just keeping the first three leading terms of the expansion in Eq. (1). As the figure shows, this prediction begins to fail for small values of  $Q$  but is off only by a few percent even at  $Q = 2$ .

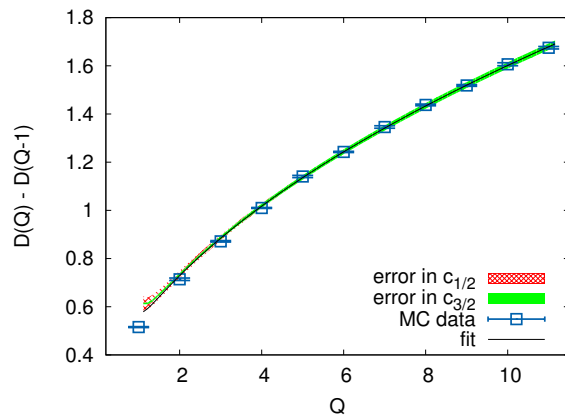


FIG. 3. Plot of  $D(Q) - D(Q-1)$  extracted using Monte Carlo calculations, along with a plot of Eq. (1) keeping the first three non-zero coefficients estimated using our fits.

Next we explore if we can connect our calculations of  $c_{\frac{3}{2}}$  and  $c_{\frac{1}{2}}$  with the ones appearing in Eq. (3) for the expansion of the energy on a torus. Calculations on the lattice with spatial lattice spacing  $a$  naturally lead to a torus geometry if in the continuum limit we can keep the physical length  $L$  fixed while taking the number of lattice points in each direction,  $L/a \rightarrow \infty$ . The lattice spacing itself is defined by setting the lattice energy  $E^L(Q)$  to be equal to the continuum energy  $E_{T^2}(Q)$  on the torus of side  $L$  as the continuum limit is taken. On the lattice we measure the energy in terms of the dimensionless number  $E^L(Q)a_t$  as a function of  $L/a$ , where  $a_t$  is the temporal lattice spacing which could in principle be different from  $a$  in the presence of a charge  $Q$ . Hence, by defining the normalization  $\xi = a_t/a$ , we can replace Eq. (3) by an equivalent formula

$$(E^L(Q)a_t)(L/a) = \xi Q^{3/2} \left( c_{\frac{3}{2}}^L + c_{\frac{1}{2}}^L Q^{-1} + c_{-\frac{1}{2}}^L Q^{-2} \dots \right) + q^L. \quad (8)$$

In this work we wish to verify Eq. (8), where in the continuum limit ( $L/a \rightarrow \infty$ ) we expect  $c_{\frac{3}{2}}^L \rightarrow c_{\frac{3}{2}}$ ,  $c_{\frac{1}{2}}^L \rightarrow c_{\frac{1}{2}}$ ,  $c_{-\frac{1}{2}}^L \rightarrow c_{-\frac{1}{2}}$  and  $q^L = -0.508$ . The normalization  $\xi$  on the other hand is a lattice-dependent constant normalization.

For a fixed lattice size  $L/a$  we can use the techniques discussed in [23] to compute energy differences  $(E^L(Q) - E^L(Q-1))a_t$ . The idea is to couple a chemical potential  $\mu_{a_t}$  to the conserved charge  $Q$  and extract the energy differences between ground states with charges  $Q$  and  $Q-1$  by tuning the chemical potential:  $\mu_c^{(Q-1)} a_t = (E^L(Q) - E^L(Q-1))a_t$ . By defining  $E^L(Q=0) = 0$  we can also extract the absolute energies which must satisfy Eq. (8). We should also keep in mind that the effective theory description is valid only when  $1 \ll L/a\sqrt{Q} \ll L/a$ . Unfortunately, our method is efficient only on small lattice sizes  $L/a$ , limiting the range of  $Q$ 's that can be used in verifying Eq. (8). In table III we list our results for  $E^L(Q)a_t(L/a)$  in the range  $1 \leq Q \leq 18$  for  $L/a = 8$  and 10.

$Q$	$E^L(Q)a_t(L/a)$ ( $L/a = 8$ )	$E^L(Q)a_t(L/a)$ ( $L/a = 10$ )	$Q$	$E^L(Q)a_t(L/a)$ ( $L/a = 8$ )	$E^L(Q)a_t(L/a)$ ( $L/a = 10$ )
1	1.3422(5)	1.3360(7)	10	39.051(4)	38.909(1)
2	3.5829(6)	3.5635(8)	11	45.054(5)	44.903(1)
3	6.4828(6)	6.4469(8)	12	51.337(5)	51.180(1)
4	9.9231(7)	9.8706(9)	13	57.886(6)	57.727(1)
5	13.832(1)	13.764(1)	14	64.691(7)	64.533(1)
6	18.161(2)	18.076(1)	15	71.742(8)	71.587(3)
7	22.875(2)	22.774(1)	16	79.028(8)	78.882(5)
8	27.944(3)	27.826(1)	17	86.541(9)	86.410(6)
9	33.343(3)	33.211(1)	18	-	94.162(7)

TABLE III. Values of  $E^L(Q)a_t(L/a)$  obtained on the lattice using the Monte Carlo method for various values of  $Q$  on lattice sizes  $L/a = 8$  and 10.

We find that our entire data in range  $4 \leq Q \leq 18$  can be

fit to the form in Eq. (8) with an acceptable  $\chi^2/DOF$  if we allow for a  $c_{-\frac{1}{2}}^L$  coefficient. However, except for the first coefficient all other coefficients fluctuate wildly as  $L/a$  changes from 8 to 10. On the other hand, if we assume that only the coefficient  $c_{-\frac{1}{2}}^L$  can depend on  $L/a$  and fix the remaining coefficients to their continuum values (*i.e.*,  $c_{\frac{3}{2}}^L = 1.194$ ,  $c_{\frac{1}{2}}^L = 0$  and  $q^L = -0.508$ ) we get a good fit for the data in the range  $12 \leq Q \leq 18$  with  $\xi = 1.03(1)$ ,  $c_{-\frac{1}{2}}^L = 1.45(10)$  for  $L/a = 8$  and  $c_{-\frac{1}{2}}^L = 1.00(5)$  for  $L/a = 10$ . This is consistent with the expectation that  $c_{-\frac{1}{2}}^L$  vanishes in the continuum limit ( $L/a \rightarrow \infty$ ) since it must be proportional to  $R^2$  [15]. In Fig. 4 we show the goodness of our estimation for the entire range of  $Q$ 's if we set  $\xi = 1.03$ ,  $c_{-\frac{1}{2}} = 0$  and  $c_{-\frac{1}{2}} = 1$  for  $L/a = 10$ . As with  $D(Q)$ , without higher coefficients the fits begin to fail for smaller values of  $Q$  but not by much until around  $Q=2$  if we include  $c_{-\frac{1}{2}}$  in the fits.

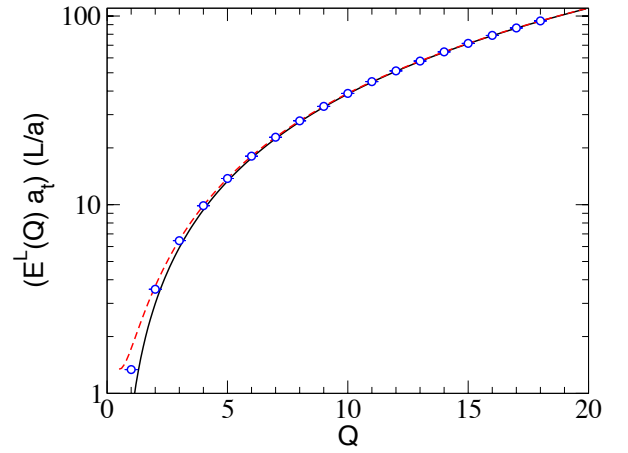


FIG. 4. The plot of  $E^L(Q)a_t(L/a)$  for  $L/a = 10$  given in table III as a function of  $Q$  along with a plot of Eq. (8) in its continuum form with  $\xi = 1.03$  and  $c_{-\frac{1}{2}}^L = 0$  (solid line) and  $c_{-\frac{1}{2}}^L = 1$  (dashed line). The y-axis is shown on a logarithmic scale to expose the goodness of Eq. (8) in determining the energies up to small values of  $Q$ .

To summarize, in this work we have developed an efficient Monte Carlo method that helps us compute the conformal dimensions  $D(Q)$  for large values of  $Q$ . We were also able to provide some evidence that connections of  $D(Q)$  with the energies  $E(Q)$  on a torus arises consistently as one expects from an effective field theory description. Thus, our results suggest that the large- $Q$  expansion may be a useful way to understand strongly-coupled systems. Using the state-operator correspondence one may be able compute universal quantities reliably, and developing Monte Carlo methods that work reliably for large- $Q$  would be very useful.

We wish to thank Uwe-Jens Wiese for helpful conversations. D.O. would like to thank Antonio Amariti, Simeon Hellerman, Orestis Loukas and Susanne Reffert for enlightening discussions and comments. D.B. would like to thank Martin Hasenbusch, Ferenc Niedermayer, Rainer Sommer and Ulli Wolff for useful discussions. The material presented here is based upon work supported by the U.S. Department of Energy, Office of Science, Nuclear Physics program under Award Number DE-FG02-05ER41368.

---

\* [debasish.banerjee@desy.de](mailto:debasish.banerjee@desy.de)

† [sch@phy.duke.edu](mailto:sch@phy.duke.edu)

‡ [dorlando@itp.unibe.ch](mailto:dorlando@itp.unibe.ch)

- [1] J. Cardy, in *Les Houches Summer School: Session 89: Exact Methods in Low-Dimensional Statistical Physics and Quantum Computing Les Houches, France, June 30-August 1, 2008* (2008) [arXiv:0807.3472 \[cond-mat.stat-mech\]](#).
- [2] J. M. Maldacena, *Int. J. Theor. Phys.* **38**, 1113 (1999), [Adv. Theor. Math. Phys.2,231(1998)], [arXiv:hep-th/9711200 \[hep-th\]](#).
- [3] A. B. Zamolodchikov, *JETP Lett.* **43**, 730 (1986), [*Pisma Zh. Eksp. Teor. Fiz.*43,565(1986)].
- [4] A. Pelissetto and E. Vicari, *Phys. Rept.* **368**, 549 (2002), [arXiv:cond-mat/0012164 \[cond-mat\]](#).
- [5] R. Rattazzi, V. S. Rychkov, E. Tonni, and A. Vichi, *JHEP* **12**, 031 (2008), [arXiv:0807.0004 \[hep-th\]](#).
- [6] M. Campostrini, M. Hasenbusch, A. Pelissetto, P. Rossi, and E. Vicari, *Phys. Rev. B* **63**, 214503 (2001), [arXiv:cond-mat/0010360 \[cond-mat\]](#).
- [7] M. Campostrini, M. Hasenbusch, A. Pelissetto, P. Rossi, and E. Vicari, *Phys. Rev. B* **65**, 144520 (2002), [arXiv:cond-mat/0110336 \[cond-mat\]](#).
- [8] M. Schuler, S. Whitsitt, L.-P. Henry, S. Sachdev, and A. M. Läuchli, *Phys. Rev. Lett.* **117**, 210401 (2016).
- [9] S. Whitsitt, M. Schuler, L.-P. Henry, A. M. Läuchli, and S. Sachdev, (2017), [arXiv:1701.03111 \[cond-mat.str-el\]](#).
- [10] J. L. Cardy, *J. Phys.* **A17**, L385 (1984).
- [11] J. L. Cardy, *J. Phys.* **A18**, L757 (1985).
- [12] S. Hellerman, D. Orlando, S. Reffert, and M. Watanabe, *JHEP* **12**, 071 (2015), [arXiv:1505.01537 \[hep-th\]](#).
- [13] L. Alvarez-Gaume, O. Loukas, D. Orlando, and S. Reffert, *JHEP* **04**, 059 (2017), [arXiv:1610.04495 \[hep-th\]](#).
- [14] A. Monin, D. Pirtskhalava, R. Rattazzi, and F. K. Seibold, (2016), [arXiv:1611.02912 \[hep-th\]](#).
- [15] O. Loukas, (2016), [arXiv:1612.08985 \[hep-th\]](#).
- [16] S. Hellerman, N. Kobayashi, S. Maeda, and M. Watanabe, (2017), [arXiv:1705.05825 \[hep-th\]](#).
- [17] S. Hellerman, S. Maeda, and M. Watanabe, (2017), [arXiv:1706.05743 \[hep-th\]](#).
- [18] O. Loukas, D. Orlando, and S. Reffert, to appear (2017).
- [19] A. Monin, *Phys. Rev. D* **94**, 085013 (2016), [arXiv:1607.06493 \[hep-th\]](#).
- [20] M. Bordag, G. L. Klimchitskaya, U. Mohideen, and V. M. Mostepanenko, *Advances in the Casimir effect*, Vol. 145 (2009) pp. 1–768.
- [21] M. Hasenbusch and E. Vicari, *Phys. Rev. B* **84**, 125136 (2011).
- [22] U. Wolff, *Phys. Rev. Lett.* **62**, 361 (1989).
- [23] D. Banerjee and S. Chandrasekharan, *Phys. Rev. D* **81**, 125007 (2010).
- [24] P. Calabrese, A. Pelissetto, and E. Vicari, *Phys. Rev. B* **67**, 054505 (2003), [arXiv:cond-mat/0209580 \[cond-mat\]](#).
- [25] M. De Prato, A. Pelissetto, and E. Vicari, *Phys. Rev. B* **68**, 092403 (2003), [arXiv:cond-mat/0302145 \[cond-mat\]](#).
- [26] J. M. Carmona, A. Pelissetto, and E. Vicari, *Phys. Rev. B* **61**, 15136 (2000), [arXiv:cond-mat/9912115 \[cond-mat\]](#).
- [27] F. Kos, D. Poland, D. Simmons-Duffin, and A. Vichi, *JHEP* **11**, 106 (2015), [arXiv:1504.07997 \[hep-th\]](#).



## SUPPLEMENTARY MATERIAL: THE ALGORITHM

As explained in [23], we can construct a worm algorithm to compute quantities in statistical mechanics, starting with the classical action

$$S([\theta]) = -\beta \sum_{x,\alpha} \cos(\theta_x - \theta_{x+\hat{\alpha}}). \quad (9)$$

We first use the identity

$$\exp\{\beta \cos \theta\} = \sum_{k=-\infty}^{\infty} I_k(\beta) e^{ik\theta}, \quad (10)$$

on each bond  $(x, \alpha)$  to integrate out the field variables  $(\theta_x)$  from the partition function

$$Z = \int [d\theta_x] e^{-S([\theta])}, \quad (11)$$

and express it in terms of a configuration of integer bond variables  $k_{x,\alpha}$ , each of which is an integer valued worldline variable denoting the charge flowing on the bond  $(x, \alpha)$ , from  $x$  to  $(x + \hat{\alpha})$ . The function  $I_k(\beta)$  is the modified Bessel function of the first kind. In terms of worldline configurations  $[k]$ , the partition function looks like

$$Z = \sum_{[k]} \prod_{x,\alpha} \{I_{k_{x,\alpha}}(\beta)\} \prod_x \delta\left(\sum_{\alpha} (k_{x,\alpha} - k_{x-\hat{\alpha},\alpha})\right). \quad (12)$$

We can use the standard worm algorithm to update worldline configurations  $[k]$  as follows:

1. We pick a random site on the lattice,  $x = x_h$  and refer to it as the head site. At the beginning we also define the tail site to be the same as the head site,  $x_t = x_h$ .
2. We randomly pick one of the  $2d$  neighbors  $x_t + \hat{\alpha}$ ,  $\alpha = \pm 1, \pm 2, \dots, \pm d$ .
3. Let  $k$  be the current on the bond joining  $x_t$  and  $x_t + \hat{\alpha}$ . If  $\alpha > 0$ , we update the forward current from  $k$  to  $k + 1$  with probability  $I_{k+1}(\beta)/I_k(\beta)$ . If this update is accepted, then we change the tail site from  $x_t \rightarrow x_t + \hat{\alpha}$ . If  $\alpha < 0$ , then with probability  $I_{k-1}(\beta)/I_k(\beta)$ , we update  $k$  to  $k - 1$  and set  $x_t \rightarrow x_t + \hat{\alpha}$ . When the updates are not accepted,  $x_t$  remains the same.
4. If the tail site  $x_t$  reaches the head site  $x_h$  the worm update ends. Otherwise, we go back to step 2.

In the above update, when we start we introduce a single positive charge at  $x_h$  and a single negative charge at  $x_t$ . During the worm update the tail site  $x_t$  moves around the lattice until it comes back and annihilates with the

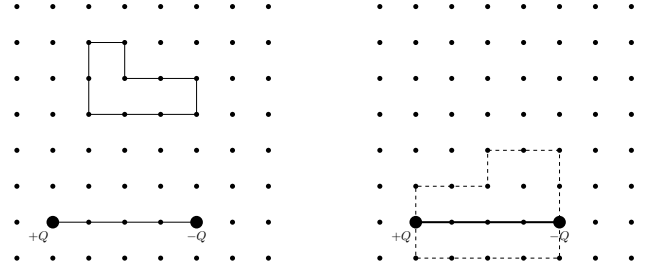


FIG. 5. (left) A standard worm update which updates the background together with a source  $Q$  and sink  $-Q$  at a fixed distance apart, (right) an example measurement update.

head site. However, at each of the intermediate steps the worm update samples the two-point correlation function  $C_1(x_t, x_h) = \langle e^{i\theta_{x_h}} e^{-i\theta_{x_t}} \rangle$ .

We can easily adapt the worm algorithm to measure the two point correlation function  $C_Q(r) = \langle e^{iQ\theta_0} e^{-iQ\theta_r} \rangle$ . We simply introduce charge  $Q$  at the head site and a charge  $-Q$  at the tail site by updating the bonds by changing  $k$  to  $k \pm Q$  as we move. Whenever the tail reaches the site  $x_t = x_h + r$ , we get a contribution to  $C_Q(r)$ . Combining this with the standard worm algorithm we can in principle get an ergodic algorithm. However, such an algorithm leads to a severe signal-to-noise problem, since the updates of  $k$  to  $k \pm Q$  is extremely inefficient especially for large  $Q$ . To solve this problem we focus on the ratio of correlation functions

$$R(r) = \frac{C_{Q+1}(r)}{C_Q(r)} = \frac{Z_{Q+1,r}}{Z_{Q,r}}, \quad (13)$$

where we define

$$Z_{Q,r} = \sum_{[k]} \prod_{x,\alpha} \{I_{k_{x,\alpha}}(\beta)\} \prod_x \delta\left(\sum_{\alpha} (k_{x,\alpha} - k_{x-\hat{\alpha},\alpha}) - Q_x\right), \quad (14)$$

with  $Q_x = Q(\delta_{x,0} - \delta_{x,r})$ . In other words  $Z_{Q,r}$  is a partition function with a charge  $Q$  fixed at  $x = 0$  and  $-Q$  at  $x = r$ . Note that we can also write the above ratio slightly differently as

$$R(r) = \langle e^{i\theta_r} e^{-i\theta_0} \rangle_{Q,r}, \quad (15)$$

where the expectation value on the right is now taken in the distribution of  $[k]$  according to the partition function  $Z_{Q,r}$ . In this case the standard worm algorithm can be used to update the configurations  $[k]$  associated with  $Z_{Q,r}$ , which we refer to as the target ensemble. In Fig. 5 (left) we show an illustration of a configuration in the target ensemble with a worm loop that updates the background configuration. In addition to the standard algorithm, we construct a special measurement algorithm where the worm update starts and ends at  $x_h = 0$ . If during this

measurement update the tail site touches reaches the site  $x_t = r$  we count it as a contribution to the ratio  $R(r)$ . More concretely,

1. We start with a configuration which has  $Q$  charges at site  $(0,0,0)$  and  $-Q$  charge at site  $(r,0,0)$ , and initialize a counter  $c = 0$ .
2. We begin a worm update with the head at  $x_h = (0,0,0)$ . We also define the tail site as  $x_t = x_h$ .
3. We pick one of the  $2d$  neighbors of  $x_t$ , and propagate the tail site using the standard worm update described earlier.
4. Whenever  $x_t = (r,0,0)$ , we increment the counter  $c = c + 1$ . This implies that the configuration generated contributes to the ratio  $R(r)$ .
5. When the tail site returns to the head site the update ends.

An illustration of this measurement update is shown in Fig. 5 (right), where the worm starts from  $x_h = 0$  and

passes through  $x_t = r$  before closing.  $R(r)$  is computed as an average of the value of  $c$  measured for each measurement worm algorithm. The actual algorithm involves several standard worm updates and an equal number of measurement updates.

For our simulations, we work at several finite cubic volumes with linear size  $L$  and compute the correlation ratios with  $r = L/2$ . In this calculation, the flux from charge  $Q$  can reach the sink either directly through the bulk or through the boundary. We can define a winding number  $w$  for each configuration  $[k]$  as the number of flux lines that reach the sink through the boundary. Then the remaining  $Q - w$  flux lines reach through the bulk. We have discovered that the value of  $R(r)$  is sensitive to  $w$ . In our work we sample all possible windings distributed according to  $Z_{Q,r}$ . On an average we see that  $w = Q/2$ . The standard worm algorithm is able to change the winding number  $w$  quite efficiently.